

# Supporting Information

## “Dielectric effects on ion transport in polyelectrolyte brushes”

Jiaxing Yuan,<sup>†,‡,⊥</sup> Hanne S. Antila,<sup>¶,⊥</sup> and Erik Luijten<sup>\*,¶,§,||,‡</sup>

<sup>†</sup>*School of Physics and Astronomy, Shanghai Jiao Tong University, Shanghai 200240, China*

<sup>‡</sup>*Institute of Natural Sciences, Shanghai Jiao Tong University, Shanghai 200240, China*

<sup>¶</sup>*Department of Materials Science and Engineering, Northwestern University, Evanston, Illinois 60208, USA*

<sup>§</sup>*Department of Engineering Sciences and Applied Mathematics, Northwestern University, Evanston, Illinois 60208, USA*

<sup>||</sup>*Department of Physics and Astronomy, Northwestern University, Evanston, Illinois 60208, USA*

<sup>⊥</sup>*These authors contributed equally.*

E-mail: [luijten@northwestern.edu](mailto:luijten@northwestern.edu)

We simulate 16 chains that are grafted in a square array and periodically replicated along the  $x$ - and  $y$ -directions. The system (main text Figure 1) has dimensions  $[0, L] \times [0, L] \times [0, L_z]$ , where  $L$  is adjusted to vary the grafting density and  $L_z = 12.5\sigma$ . The actual simulation cell extends from  $z = -L_z$  to  $z = L_z$  to accommodate the image charges. Electrostatic interactions are calculated via a modified three-dimensional particle–particle particle–mesh algorithm<sup>1</sup> with relative accuracy  $10^{-5}$ . Artifacts owing to the periodicity in the  $z$ -direction are suppressed by adding a  $4L_z$ -thick vacuum layer and a dipole correction.<sup>2</sup> We confirmed that this reduces the systematic relative root-mean-square error in the force on each ion to less than  $10^{-7}$ , significantly smaller than

the precision of the electrostatic solver. The solvent viscosity opposing the ion motion is captured by a Langevin thermostat with damping time  $1.0\tau$ , where  $\tau = (m\sigma^2/\varepsilon_{\text{LJ}})^{1/2}$  is the LJ unit of time. We equilibrate the system for  $10^6$  steps (of length  $0.01\tau$ ) after which we continue with production runs for  $10^8$  steps, corresponding to  $5.6\ \mu\text{s}$ . By comparison, the long runs for simple electrolytes in Ref. 3 correspond to  $0.056\ \text{ms}$  (not  $5.6\ \text{ms}$  as erroneously stated). Simulations were conducted using a version of LAMMPS<sup>4</sup> that was modified to account for image charges.

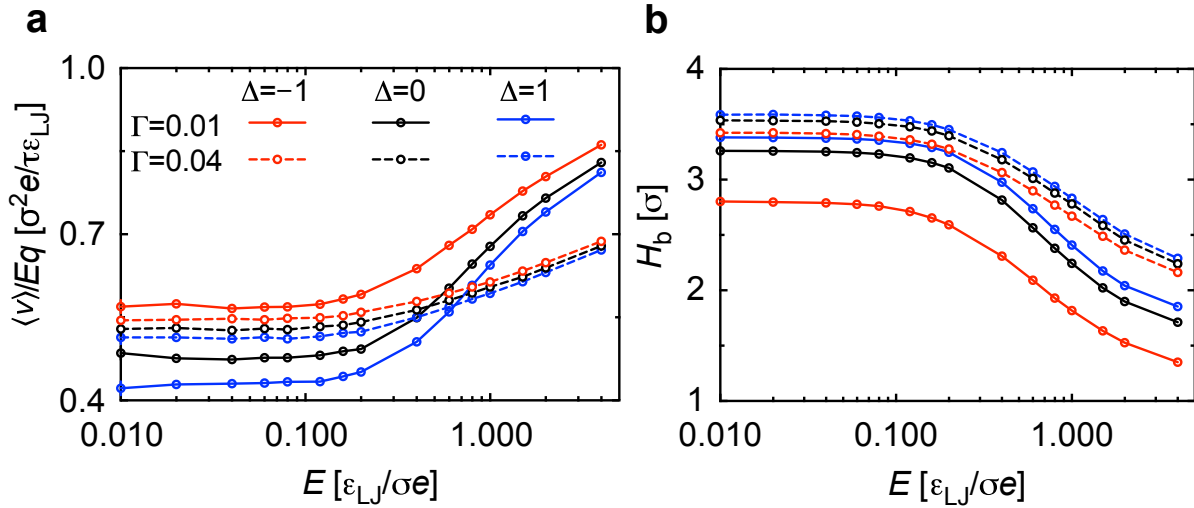


Figure S1: Ion transport and brush structure as a function of external driving field. (a) Ion mobility  $\mu$  and (b) brush distribution height  $H_b$  as a function of field strength  $E$  for grafting densities  $\Gamma = 0.01\sigma^{-2}$  and  $\Gamma = 0.04\sigma^{-2}$ . This illustrates that the electric field  $E = 0.02\varepsilon_{\text{LJ}}/(\sigma e)$  employed in the main text lies within the linear-response regime, where the polymer structure is nearly unaffected by the applied field.

Figure S1 presents the ion mobility  $\mu = \langle v \rangle / (Eq)$  and the brush height  $H_b = (\int_0^{L_z} \rho_b(z) z dz) / (\int_0^{L_z} \rho_b(z) dz)$  as a function of the external electric field  $E$ . As the field strength is increased, the ion response becomes nonlinear. Both the onset and the magnitude of this nonlinearity depend on brush grafting density, with a slightly earlier and stronger deviation for a sparse brush, where ion transport is dominated by electrostatic ion–polymer binding. A sparse brush is also capable of larger deformation under an external field, as reflected in the more pronounced response of the brush structure (Figure S1b), which in turn also affects ion response. Based on these data, we choose to utilize a low driving field of magnitude  $E = 0.02\varepsilon_{\text{LJ}}/(\sigma e)$  to obtain the results presented in the main text.

Figure S2 summarizes how the effects of surface polarization on ion mobility (top row), counterion distribution (middle row), and monomer distribution (bottom row) change when the brush grafting density  $\Gamma$  is varied. The counterion distributions and the polymer distributions are normalized (unlike in Figure 3b in the main text) to illustrate the relative magnitude of the dielectric effects at different  $\Gamma$ .

For all the quantities presented in Figures S2, both the magnitude and range (in terms of distance to the substrate) of the dielectric modulation are reduced when  $\Gamma$  is increased. This can be understood from the increase in electrostatic screening at larger  $\Gamma$ . This screening, along with the decreased importance of electrostatic interactions for ion transport at high  $\Gamma$ , explains why the ion mobilities become independent of substrate permittivity in dense brushes (Figure 3a, main text).

The relative magnitude of the perturbation caused by substrate permittivity on local mobility (Figure S2, top) is always comparable for  $\Delta = -1$  and  $\Delta = 1$ . This indicates that the stronger modulation of the average ion mobilities (Figure 3a, main text) by a conducting substrate must stem from the build-up of ions owing to the attractive polarization.

Unlike the comparable modulation of local mobilities for  $\Delta = \pm 1$ , the dielectric effect on the spatial distribution of charge is strongly asymmetric. A high-permittivity substrate causes a more pronounced change in both the ion and the polymer distributions than a low-permittivity substrate. The polymer distribution (Figure S2, bottom row) reveals that this originates from the grafting of the polymers to the interface: the monomers cannot be fully repelled by the insulating substrate—a constraint which then propagates to the ion distribution (Figure S2, middle row) via ion–monomer binding (the results shown are obtained at Manning parameter  $\xi \approx 2.67$ ). Note that the comparable modulation of local mobilities for  $\Delta = \pm 1$  also indicates that the small modifications of polymer and ion densities caused by the surface polarization are not strong enough to have an effect on the mobilities via electrostatic screening or steric effects.

Above (Figure S2) and in the main text Figure 3a, we have truncated the mobility and distribution profiles at the distance  $z = 3\sigma$  to focus on the dielectric effects occurring at the interface. The profiles with the full  $z$ -range are presented in Figure S3 for the same system as in Figure 3b in

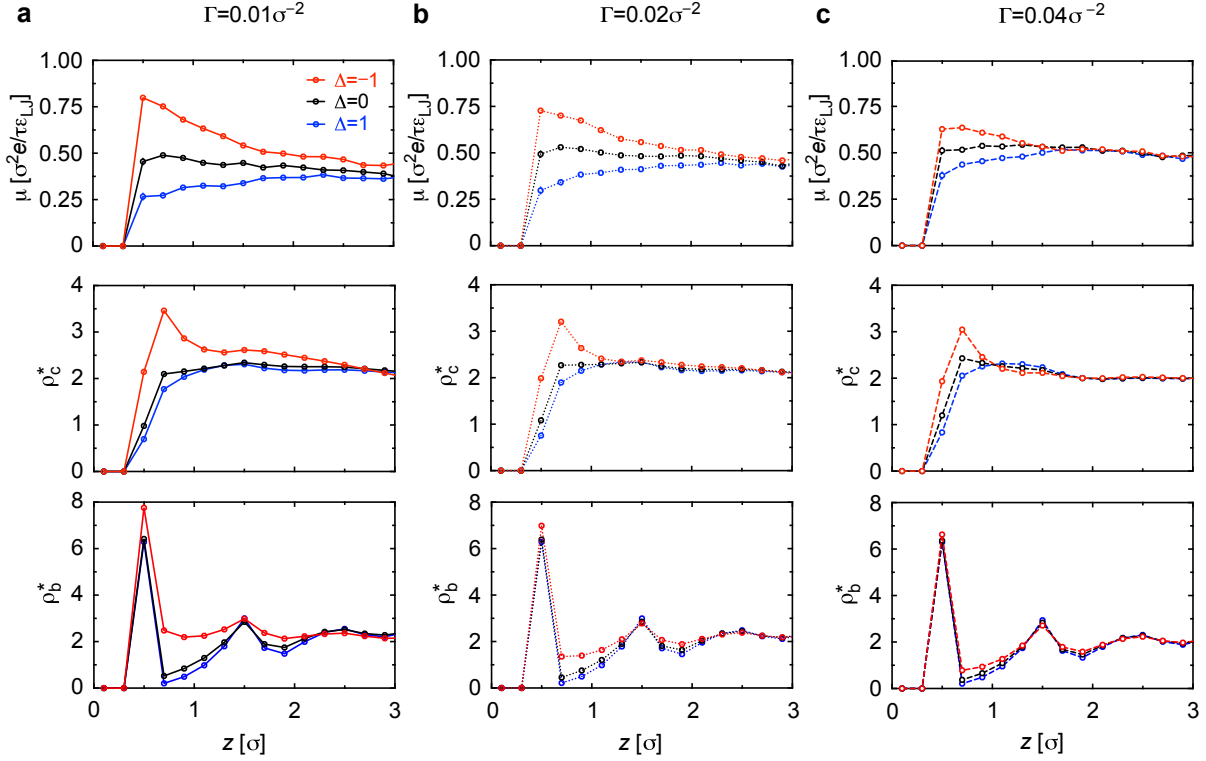


Figure S2: Range and magnitude of the dielectric effects for different grafting densities. Ion mobility  $\mu$ , normalized counterion density distribution  $\rho_c^*$  (rescaled by the overall counterion density), and normalized brush monomer density distribution  $\rho_b^*$  (rescaled by the overall monomer density) are presented as a function of the distance to the substrate for grafting densities (a)  $\Gamma = 0.01\sigma^{-2}$ , (b)  $\Gamma = 0.02\sigma^{-2}$ , and (c)  $\Gamma = 0.04\sigma^{-2}$ . The effect of the substrate permittivity on local mobilities is almost equally strong for  $\Delta = -1$  and  $\Delta = 1$ , whereas the effect on local ion and polymer densities is much stronger for  $\Delta = -1$  than for  $\Delta = 1$ . As grafting density increases, the dielectric modulation of all quantities presented diminishes due to electrostatic screening.

the main text. After  $z = 3\sigma$  the ion mobility exhibits a gradual increase as the polymer density decreases (Figure S3 middle) such that both the electrostatic ion–polymer binding and the steric effects are weakened. As the data is obtained in the regime of strong interactions (Manning parameter  $\xi = 2.67$ ), the ion density (Figure S3 bottom) follows the monomer distribution and relatively few ions reside outside of the brush. These ions experience free conduction and the ion mobility hence reaches a maximum outside of the brush.

Figure S4 summarizes the effects of changing the Manning parameter  $\xi = l_B\lambda$  on ion mobility, brush structure, and ion flux. We vary  $\xi$  either by changing  $l_B$  (variation of solvent permittivity or temperature) or by scaling the monomer charges (variation of  $\lambda$ ). The functional dependence of

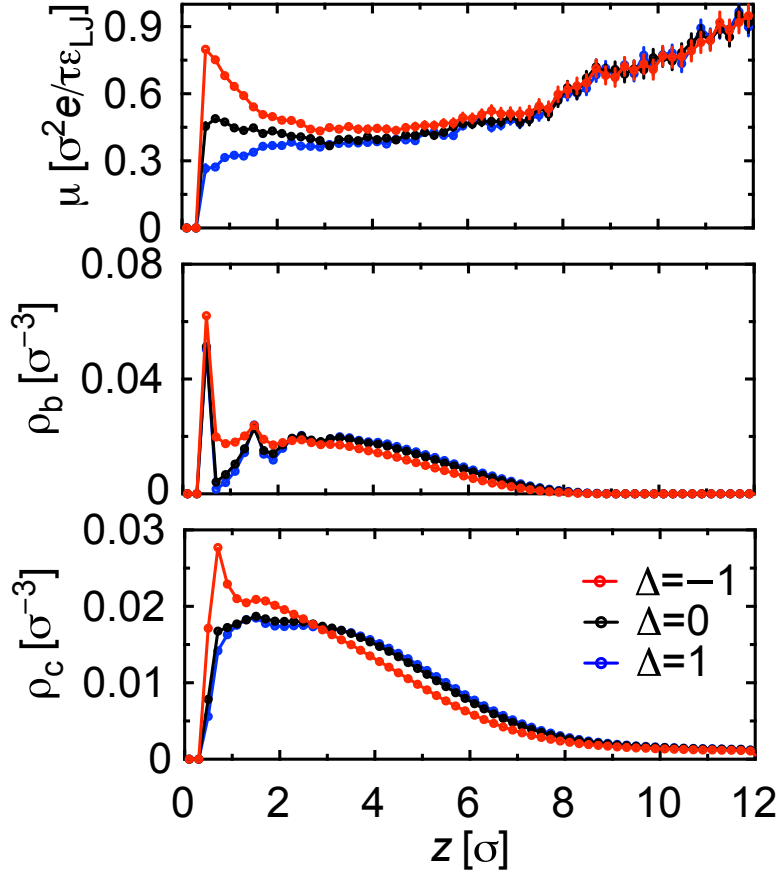


Figure S3: Ion mobility  $\mu$  (top), brush monomer density  $\rho_b$  (middle), and ion density  $\rho_c$  (bottom) profiles as a function of distance  $z$  to the substrate for brushes with grafting density  $\Gamma = 0.01\sigma^{-2}$ .

brush height on Manning parameter is qualitatively different for the two approaches (both scenarios have been reported separately, but appear not to have been compared before). Upon increasing Bjerrum length we observe an initial expansion followed by a contraction above  $\xi^* \approx 1$  as Manning condensation of ions onto the brush screens the intra- and inter-polymer repulsion<sup>5</sup> (Figure S4a, top). Conversely, increasing  $\xi$  via  $\lambda$  leads to monotonic expansion of the brush even though ion adsorption is still observed (Figure S4b, top). This expansion occurs because the intra- and inter-polymer repulsions scale as  $\lambda^2$  and hence dominate over the polymer–ion attractions scaling as  $\lambda$  (cf. Ref. 6).

Even though the brush conformation and ion distribution depend on the manner in which  $\xi$  is tuned, the resulting ion mobilities are very similar (Figure S4a,b, middle panels), showing the same strong decrease with increasing  $\xi$ . As Manning condensation increases, more ions migrate into the brush and ion–polymer binding is enhanced. However, the overall ion *flux*  $\Phi$  is vastly

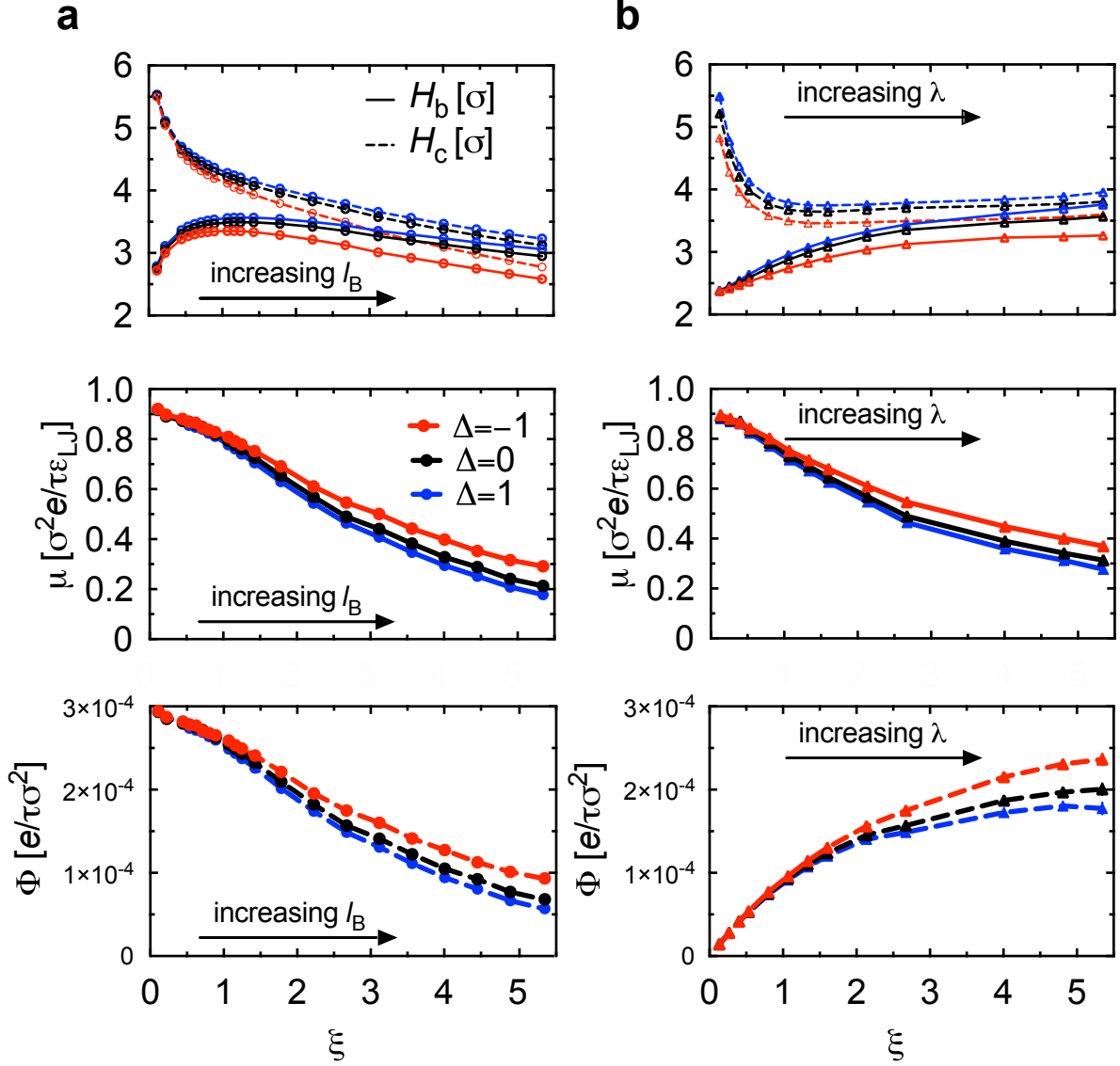


Figure S4: Brush structure, the average ion mobility, and the average ion flux, as well as the degree to which they are affected by substrate permittivity, all depend on electrostatic coupling, quantified here by the Manning parameter  $\xi$ . We vary  $\xi$  by (a) tuning Bjerrum length ( $\epsilon_{\text{sol}}$  or  $T$ ) or (b) linear polymer charge density, and show (top) brush distribution height  $H_b = (\int_0^{L_z} \rho_b(z) z dz) / (\int_0^{L_z} \rho_b(z) dz)$  and counterion distribution height  $H_c = (\int_0^{L_z} \rho_c(z) z dz) / (\int_0^{L_z} \rho_c(z) dz)$ , (middle) ion mobility  $\mu$ , and (bottom) ion flux  $\Phi = \rho q \langle v \rangle$ , at  $\Gamma = 0.02 \sigma^{-2}$ . Here  $\rho_b$  and  $\rho_c$  denote the monomer and counterion distributions, respectively, and  $\rho$  is the overall counterion density.

different in the two scenarios. An increase in Bjerrum length reduces the flux proportionally to the mobility, but an increase in polymer charge implies a growth in the number of counterions that overwhelms the reduction in mobility (Figure S4a,b, bottom panels). Indeed, this is reflected in the experimentally well-established enhancement of conductivity in PEB-functionalized nanochannels

upon protonation of the polyelectrolytes.<sup>7,8</sup>

In this work, we have focused on salt-free systems with short polymers. When the amount of charge in the system is increased, either by introducing longer polymers or by addition of salt, both the balance between electrostatic ion binding and steric effects that governs ion conduction and the magnitude of dielectric effects will be altered by the increased electrostatic screening. However, the mechanisms observed will remain valid. We anticipate them to be particularly relevant for nanofluidic devices where interfacial phenomena are enhanced by the large surface-to-volume ratio and where precise control over ionic mobilities becomes increasingly important.

The simulations presented ignore hydrodynamic effects beyond the Langevin thermostat. Such effects are expected to be less important in dilute conditions. In fact, previous simulations of simple electrolytes<sup>9</sup> have shown that even at 1.0 M KCl, hydrodynamic effects enhance the diffusion coefficient of  $K^+$  only by  $\sim 3\%$ . As this concentration approximately corresponds to a brush with higher grafting density than what was studied here, we don't expect hydrodynamic interactions to drastically alter the ionic velocities in the hopping process.

In addition, the coarse-grained model lacks a description of the molecular structure of the solvent, and thus does not capture effects such as the formation of an enhanced hydrogen-bonding network for water within PEBs<sup>10</sup> or the emergence of an oriented hydration layer at the solid–fluid interface.<sup>11</sup> These phenomena would slow down ion transport due to hindered water diffusion and the presence of an oriented hydration layer can alter the dielectric mismatch at the interface.<sup>12,13</sup> A detailed study of these aspects will require models with explicit water. Despite the simplifications in the current model, we consider the mechanisms uncovered here as fundamental to understanding ion transport in media where one of the charged components is immobilized and where the structure and interactions are modulated by a polarizable interface.

## References

- (1) Yuan, J.; Antila, H. S.; Luijten, E. Particle–particle particle–mesh algorithm for electrolytes between charged dielectric interfaces. 2018; submitted.
- (2) Yeh, I.-C.; Berkowitz, M. L. Ewald summation for systems with slab geometry. *J. Chem. Phys.* **1999**, *111*, 3155–3162.
- (3) Antila, H. S.; Luijten, E. Dielectric modulation of ion transport near interfaces. *Phys. Rev. Lett.* **2018**, *120*, 135501.
- (4) Plimpton, S. J. Fast parallel algorithms for short-range molecular dynamics. *J. Comp. Phys.* **1995**, *117*, 1–19.
- (5) Hehmeyer, O. J.; Arya, G.; Panagiotopoulos, A. Z.; Szleifer, I. Monte Carlo simulation and molecular theory of tethered polyelectrolytes. *J. Chem. Phys.* **2007**, *126*, 244902.
- (6) Ouyang, H.; Xia, Z.; Zhe, J. Static and dynamic responses of polyelectrolyte brushes under external electric field. *Nanotech.* **2009**, *20*, 195703.
- (7) Yameen, B.; Ali, M.; Neumann, R.; Ensinger, W.; Knoll, W.; Azzaroni, O. Synthetic proton-gated ion channels via single solid-state nanochannels modified with responsive polymer brushes. *Nano Letters* **2009**, *9*, 2788–2793.
- (8) Yameen, B.; Ali, M.; Neumann, R.; Ensinger, W.; Knoll, W.; Azzaroni, O. Single conical nanopores displaying pH-tunable rectifying characteristics. Manipulating ionic transport with zwitterionic polymer brushes. *J. Am. Chem. Soc.* **2009**, *131*, 2070–2071.
- (9) Jardat, M.; Bernard, O.; Turq, P.; Kneller, G. R. Transport coefficients of electrolyte solutions from Smart Brownian dynamics simulations. *J. Chem. Phys.* **1999**, *110*, 7993–7999.
- (10) Yamazoe, K.; Higaki, Y.; Inutsuka, Y.; Miyawaki, J.; Cui, Y.-T.; Takahara, A.; Harada, Y. Enhancement of the hydrogen-bonding network of water confined in a polyelectrolyte brush. *Langmuir* **2017**, *33*, 3954–3959.

- (11) Qiao, R.; Aluru, N. R. Atomistic simulation of KCl transport in charged silicon nanochannels: Interfacial effects. *Colloids Surf. A* **2005**, *267*, 103–109.
- (12) Bonthuis, D. J.; Gekle, S.; Netz, R. R. Dielectric profile of interfacial water and its effect on double-layer capacitance. *Phys. Rev. Lett.* **2011**, *107*, 166102.
- (13) Fumagalli, L.; Esfandiar, A.; Fabregas, R.; Hu, S.; Ares, P.; Janardanan, A.; Yang, Q.; Radha, B.; Taniguchi, T.; Watanabe, K.; Gomila, G.; Novoselov, K. S.; Geim, A. K. Anomalous low dielectric constant of confined water. *Science* **2018**, *360*, 1339–1342.